REPORT DOCUMENTATION

AD-A281 470

Approved
No 0704-0188

1. AGENCY USE ONLY (Leave blank)	2. REPORT DATE	3. REPORT TYPE AND DATES COVERED
	28 March 1994	Final Report, 1 Aug 1990- 31 Jan. 1994

4. TITLE AND SUBTITLE
Electromagnetic Processing of Refractory Metal Silicide/Oxide Composites

5. FUNDING NUMBERS
DAAL03-90-G-0194

6. AUTHOR(S)
Arturo Bronson and Joseph Pierluissi

7. PERFORMING ORGANIZATION NAME(S) AND ADDRESS(ES)
Departments of Metallurgical and Materials Engineering
and Electrical Engineering
University of Texas at El Paso
El Paso, Texas 79968

8. PERFORMING ORGANIZATION REPORT NUMBER

9. SPONSORING/MONITORING AGENCY NAME(S) AND ADDRESS(ES)
U.S. Army Research Office
P. O. Box 12211
Research Triangle Park, NC 27709-2211

10. SPONSORING/MONITORING AGENCY REPORT NUMBER
ARO 28198.1-MS-SDI

11. SUPPLEMENTARY NOTES
The views, opinions and/or findings contained in this report are those of the author(s) and should not be construed as an official Department of the Army position, policy, or decision, unless so designated by other documentation.

12a. DISTRIBUTION/AVAILABILITY STATEMENT
Approved for public release; distribution unlimited.

12b. DISTRIBUTION CODE

13. ABSTRACT *(Maximum 200 words)*

The electromagnetic processing of refractory metal ceramic materials within the hot zone of an induction furnace was investigated by modeling the electromagnetic field at high temperatures (i.e., 1800°C) and by characterizing the microstructure after annealing zirconium disilicide powder which sustained the field. The finite element analysis (FEA) of the electromagnetic field within the furnace determined that the magnetic vector potential was significant just outside the center axis. The analysis also determined that the magnetic vector potential can substantially generate a temperature rise within the zirconium disilicide phase because of its conductivity at 1800°C. With ceramic powders averaging in size of 3-10μ, a reaction couple of $ZrSi/SiO_2$ was prepared in-situ and annealed at temperatures greater than 1900°C. The reaction couple developed an interdiffusion zone near the SiO_2/air interface and an inner core. Within the interdiffusion zone, reaction products consisting ZrO_2 and SiO_2 precipitates resulted from the diffusion of oxygen through a silica layer. During the annealing process, the couple's inner core consisted of ZrSi and liquid silicide, which upon solidification resulted in ZrSi, $ZrSi_2$ and a $Si/ZrSi_2$ eutectic structure.

14. SUBJECT TERMS	15. NUMBER OF PAGES
Electromagnetic, Processing, Ceramic Silicide, Zirconia, Composites	22
	16. PRICE CODE

17. SECURITY CLASSIFICATION OF REPORT	18. SECURITY CLASSIFICATION OF THIS PAGE	19. SECURITY CLASSIFICATION OF ABSTRACT	20. LIMITATION OF ABSTR
UNCLASSIFIED	UNCLASSIFIED	UNCLASSIFIED	UL

NSN 7540-01-280-5500

Standard Form 298 (Rev 2-89)
Prescribed by ANSI Std Z39-18
298-102

ELECTROMAGNETIC PROCESSING OF REFRACTORY METAL SILICIDE/OXIDE COMPOSITES

Final Report

Arturo Bronson
Department of Metallurgical and Materials Engineering

and

Joseph Pierluissi
Department of Electrical Engineering

March 28, 1994

U. S. Army Research Office

Contract No. DAAL03-90-G-0194

University of Texas at El Paso

TABLE OF CONTENTS

1. STATEMENT OF THE PROBLEM

The primary goal of the research was to study electromagnetic processing of refractory metal ceramic materials within the hot zone of an induction furnace. The materials are useful for cutting tools and structural ceramics for high temperature applications. One major task involved the modeling of the temperature and potential gradients in an electromagnetic field at high temperatures (i.e., 1800°C) by using finite element analysis. Another task investigated the electromagnetic processing of refractory metal composites (i.e., Zr-O-Si system) by experimentation.

2. INTRODUCTION

A wide variety of techniques have been adopted throughout the years to solve the electromagnetic and thermal second-order differential equations, governing the problem of the axisymmetric cylindrical induction furnace. In the present study, the authors followed the techniques of Donea, Giuliani, and Phillipe [1] in the electromagnetic analysis, and Maten and Melissen [2] in the coupled thermal problem. The basic approach consisted of initially solving the scalar, inhomogeneous diffusion equation for the magnetic vector potential, and, consequently seek a solution to the heat equation to acquire the temperature distribution. On electrically conducting materials, the magnetic vector potential induces eddy currents which, in turn, generate heat, thus raising the material's temperature. The finite element method possesses attractive advantages of easily accommodating the arbitrary configurations, a wide variety of material properties, and the full range of electromagnetic and thermal variables. However, the availability of physical properties at temperatures greater than 1000°C limits the application of finite element analysis.

Electromagnetic processing of refractory metal composites are required because of their inherent difficulty to consolidate as a result of their high melting temperatures and mechanical properties. The compatibility of the phases of boride/silicide/oxide ceramics at temperatures greater than 1600°C must be understood to improve the processing, to predict the performance during service, and to control the protective phases during oxidation. Reaction couples of zirconium disilicide and zirconia were selected for the present study, because a previous investigation determined that hafnium boride was insoluble and unreactive with either hafnium silicide or hafnia [3]. In addition, the zirconium system was used because zirconia crucibles with reproducible properties were commercially available, and the zirconium system and hafnium system are very similar. Experiments were designed to investigate the electromagnetic processing of refractory metal composites in air at 1900°C.

3. MAGNETO-THERMAL MODELING

3.1. ELECTROMAGNETIC ANALYSIS

The electromagnetic modeling of the induction furnace was accomplished through the use of variational finite elements with second-order shape functions, and a total of 60 elements representing seven regions within the induction furnace. A variety of other methods have been adopted in the past including approximate analytical techniques [4], Green's functions [5], boundary elements [6] and finite differences [7]. However, the most versatile and commonly-adopted technique is the finite element method [8]. In this latter method, the governing differential equation is the diffusion equation which in terms of the azimuthal component of the magnetic vector potential

A_ϕ becomes

$$\frac{1}{\mu}\left(\frac{\partial^2 A_\phi}{\partial r^2}+\frac{1}{r}\frac{\partial A_\phi}{\partial r}-\frac{A_\phi}{r^2}+\frac{\partial^2 A_\phi}{\partial z^2}\right)-\left(j\omega\sigma-\omega^2\varepsilon\right)A_\phi+J_o=0 \qquad (1)$$

Here, (r, ø, z) represent a point in the conventional circularly-cylindrical coordinate system, ω is the radian frequency, J_O is the source sinusoidal current density, and μ, ε, and σ are respectively the permeability, permittivity, and conductivity of the medium. Figure 1 depicts a simplified cross-sectional view along a constant z of the induction furnace showing the materials used. The solution of equation (1) and of its functional are subject to the conditions that A_ϕ be zero along the surface of the copper load coil and along the axis of revolution. Instead of working with equation (1) its variational functional [1] $F(A_\phi)$, namely

$$F(A_\phi)=\int_\Omega\left\{\frac{1}{2\mu}\left[\left(\frac{\partial A_\phi}{\partial r}\right)^2+\left(\frac{\partial A_\phi}{\partial z}\right)^2+\frac{A_\phi^{\,2}}{r^2}\right]+\frac{j\omega\sigma A_\phi^{\,2}}{2}-\frac{\omega^2\varepsilon A_\phi^{\,2}}{2}-J_o\right\}d\Omega \qquad (2)$$

$$-\int_S\frac{1}{\mu}\left(\frac{\partial A_\phi}{\partial r}\hat{n}_r+\frac{\partial A_\phi}{\mu z}\hat{n}_z\right)A_\phi dS$$

is more commonly solved when using finite elements. In equation (2), S is the surface of the shielding chamber, Ω is its interior, and $\hat{n}_r$ and $\hat{n}_z$ are unit normal vectors. In terms of matrices and after minimization, equation (2) may be written for all elements as

$$[K+L]\{A\}=[G] \qquad (3)$$

in which {A} represents the entire set of unknown values of the magnetic potential at the element nodes, and [K], [L], and [G] are element matrices involving the integrals in (2). An International Mathematical and Scientific Libraries (IMSL) subroutine was then applied to (3) to solve the resultant set of linear equations for the unknown nodal magnetic potentials.

3.2. THERMAL ANALYSIS

Maten and Melissen [2] recently reported that the differential equation in terms of the steady-state temperature distribution (T) inside an induction furnace driven by the magnetic vector potential A_ϕ is as follows:

$$-k\left(\frac{\partial^2 T}{\partial r^2}+\frac{\partial^2 T}{\partial z^2}+\frac{1}{r}\frac{\partial T}{\partial r}\right)=\frac{1}{2}\sigma\omega^2 A_\phi^{\,2}. \qquad (4)$$

where k is the thermal conductivity. Equation (4), as well as its associated functional, was solved by assuming temperatures at specific regions within the furnace and by establishing a boundary condition consistent with convective and radiative heat

transfer. The first boundary condition sets the specified temperatures as

$$\begin{aligned} T &= 300^\circ\ C, \qquad 0 \le z \le \tfrac{1}{3} l \\ T &= 400^\circ\ C, \qquad \tfrac{1}{3} l \le z \le \tfrac{2}{3} l \\ T &= 1800^\circ\ C, \qquad \tfrac{2}{3} l \le z \le l \end{aligned} \tag{5}$$

where the second may be summarized as [8]

$$k\frac{\partial T}{\partial r} = -h\left(T - T_a\right) - e\gamma\left(T^4 - T_a^{\,4}\right). \tag{6}$$

Here, T_a is the measured temperature along the surface, and h, e, and γ are, respectively, the convective heat transfer coefficient, the emissivity, and the Stefan-Boltzman constant, and l is the height of the induction furnace. The variational functional associated with the heat equation in (4) is given by [8] as

$$\begin{aligned} F(T) = \frac{1}{2}\int_{\Omega}\left\{k\left[\left(\frac{\partial T^2}{\partial r}\right)^2 + \left(\frac{\partial T}{\partial z}\right)^2\right] - \sigma\omega^2 A_\phi^{\,2}\right\} T d\Omega \\ - \int_S k\left(\frac{\partial T}{\partial r}\hat{n}_r + \frac{\partial T}{\partial z}\hat{n}_z\right) T dS\,, \end{aligned} \tag{7}$$

in which the region Ω and the surface S represent combinations of the sets described in (5). For the solution, equation (7) is minimized to obtain a matrix expansion similar to (3), but in terms of both the now known nodal magnetic vector potentials and the unknown nodal temperatures [8].

3.3. COMPUTATION

An application was made of the finite elements to the diffusion equation in equation (1) and to the heat equation in equation (4). The time-varying magnetic field was obtained by passing a current of 3.0 A at a frequency of 2.7 MHz through the coil shown in the schematic of Figure 1. The schematic also shows some of the materials used in experimentation, as well as the discretization of the induction furnace model for analysis using finite elements.

The program written for solving both set of equations for the magnetic and thermal quantities was divided into three parts, namely: preprocessor, solution, and postprocessor. The preprocessor dealt with the discretization, material properties, nodal coordinates, and node numbering. The solution component included the evaluation of the functional matrices and the solution of the resulting set of linear equations in the unknown nodal values. The postprocessor was used for calculating other physical variables and for plotting the results. Details of the respective FORTRAN, BASIC, and C++ programs may be found in Ko's [9] and Villalva's [10]

theses.

In the finite element analysis the magnetic vector potential was first obtained, and then the other desirable physical parameters were obtained either numerically from the vector potential using Maxwell's equations, or through a second finite element analysis which used the potential as a known input variable. The material characteristics of the seven regions used for this study are listed in Table 1 [11-13]. In the first case, the parameters included the magnetic flux density, electric flux density, electric scalar potential, eddy currents, as well as the gradients of the electric scalar potential and of the magnetic scalar potential. A color contour plot of the magnetic flux density is shown in Figure 2 at a temperature of 1800°C. The physical quantities included in the second case are the temperature and gradient of the temperature, as shown in Figures 3 and 4.

4. MICROSTRUCTURAL FEATURES

The sample consisted of $ZrSi_2$ enclosed in a quartz ampule, which was evacuated and heated to 1900°C. A schematic of the experimental apparatus indicating the position of the ampule and crucible is shown in Figure 5. At 1900°C, the quartz with a melting temperature of 1726°C was expected to fall to the bottom of the zirconia crucible and form a silicide melt. Although the densities for ZrO_2 and $ZrSi_2$ were not found at 1900°C, at room temperature, $ZrSi_2$ (4.88 g/cm^3) is denser than SiO_2 (2.32-2.66 g/cm^3). During the experimental run, the quartz collapsed around the $ZrSi_2$ powder and maintained the capsule's form. The cross-section of the capsule depicted an adherent silica layer surrounding a region which appeared to be molten silicide at first glance. The silica did not collapse within the internal wall of the ZrO_2 crucible. Hence, the results are given here for only the silicide contained within the quartz forming a silicide/silica reaction couple.

A typical microstructure acquired from the experimental runs, which were made at annealing times from 4 to 25 hours, is shown in Figure 6. The following sections describe and discuss interdiffusion zone and inner core acquired from the experiments. At 1900°C, an interdiffusion zone developed between the melted silicide core and the silica wall, and an internal core composed primarily of molten silicide and ZrSi precipitates. The interdiffusion zone developed distinct phases as a result of oxygen diffusion, and the core, upon cooling, developed ZrSi and $ZrSi_2$ precipitates with a eutectic structure.

The calibration of the pyrometric measurement of temperature was performed with the melting point of platinum located directly underneath the zirconia crucible, as shown in Figure 5. However, during operation of the furnace at 1900°C, a white glow suddenly would appear above the furnace chamber. The furnace voltage would also spike dramatically and result in an instability causing the furnace control circuit to terminate the experimental run. If the furnace did not power off during these temperature spikes, the zirconia crucible and the surrounding zirconia grog would sometimes melt. The finite element modeling performed by the research group determined that the silicide could create a significant temperature rise resulting from the electromagnetic field sustaining eddy currents. The effect of the electromagnetic field on the conductive silicide depends significantly on the radial position along the

furnace.

4.1. INTERDIFFUSION ZONE

To analyze the phases in the specimens, the scanning electron microscope in conjunction with energy dispersive x-ray analysis (EDXA) examined the samples after annealing. The microstructure along the silica wall after four hours annealing time contained zirconium oxide, two distinct phases of zirconium silicide, and silica. The EDXA identified two zirconium silicides present at the interface, because of unequal zirconium intensity peaks in spectra. Scanning electron micrographs also revealed a eutectic microstructure, which infer the formation of silicon and zirconium silicide. Zirconia precipitates and $ZrSi_2$ globules in a silica matrix were also found in the interdiffusion zone. The globules resulted in the immiscibility of zirconium silicide and silica, and the globules had two distinct phases (ZrSi and $ZrSi_2$) surrounded by an eutectic structure.

4.2. INTERNAL CORE

The interior of the samples had a distinctively different microstructure than the interdiffusion zone. After annealing for four hours the silica ampule contained zirconium disilicide powder, the interior showed large zirconium silicide precipitates surrounded by an eutectic microstructure. The eutectic microstructure consisted of peritectic $ZrSi_2$ precipitates and silicon. For example, after sixteen hours of annealing, the microstructure in the interior of the sample was a two phase microstructure, as shown in Figure 7. X-ray diffraction patterns indicated the presence of ZrSi, $ZrSi_2$, and ZrO_2 phases for all samples, as shown in Table 2. These patterns supported the results acquired from the EDXA, in which the spectrums had small and large peaks of silicon inferring the presence of ZrSi and $ZrSi_2$.

The phases within the inner core and the interdiffusion of the five samples differ in microstructural features, because of uncontrolled heating as a result of the silicide conductivity. For the inner core, complete melting of the $ZrSi_2$ occurred with a non-uniform distribution of precipitates across the core. The large precipitates of ZrSi ranged in lengths of 200-1600 μm and 15-110 μm wide surrounded by a eutectic microstructure. In the seven hour sample, large precipitates were found in the interior of the sample similar to a precipitate found on the globule located inside the silica wall. Each large globule has a large precipitate surrounded by a eutectic microstructure (Figure 8). The 15.9 and 25 hour samples did not have the large precipitates in their microstructure within the core region. The inconsistency in the type of microstructure developed throughout the samples was attributed to a difference in the temperature of silicide, which sustains the electromagnetic field.

4.3 SOLIDIFICATION OF INNER CORE

The formation of the phases within the inner core can be explained with the aid of the Zr-Si phase diagram [14]. At 1900°C, a two phase field composed of liquid and αZrSi exists and upon cooling, the following peritectic reaction occurs at 1620°C:

$$L + \alpha ZrSi = ZrSi_2 \qquad (8)$$

The peritectic reaction occurs sluggishly even though the non-equilibrium cooling

would drive the reaction toward $ZrSi_2$. The peritectic phase (i.e., $ZrSi_2$) was sometimes found around the $\alpha ZrSi$ precipitates, and the eutectic microstructure resulted from the residual liquid, which was deficient of zirconium. As the liquidus reaches the eutectic temperature, the following reaction results:

$$L = ZrSi_2 + Si \qquad (9)$$

Peña [15] reported that the eutectic structure infers that the solidification of the ZrSi + liquid mixture occurred to the left of the $ZrSi_2$ composition, although pure $ZrSi_2$ was originally placed within the capsule.

4.4 OXIDATION OF REACTION COUPLE

Zirconia and silica were found in the interdiffusion zone of the silicide/silica couple. At 1900°C, the capsule formed an internal core of ZrSi solid and liquid. Oxygen diffuses through the SiO_2 wall and reacts according to the following reaction:

$$ZrSi + 2O_2 = ZrO_2 + 2SiO_2 \qquad (10)$$

The presence of large precipitates and a eutectic microstructure at the interdiffusion zone resulted from the solidification of the melt similar to that of the core.

The stable phases at 1900°C are ZrSi, liquid silicide and liquid silica in the reaction couple. The oxygen reacts with the silicide to form ZrO_2. The ZrO_2-SiO_2 phase diagram [16] shows that $ZrSiO_4$ is not stable at 1900°C, and, hence, the zirconium silicate would not form. The reaction couple can be explained as pseudo-ternary of ZrSi, ZrO_2, and SiO_2 within the Zr-Si-O system at temperatures greater than the peritectic temperature (1620°C), above which the ZrSi-liquid mixture stabilizes with SiO_2. With the diffusion of oxygen through silica, ZrO_2 would form with a molar stoichiometry ratio of $ZrO_2/SiO_2 = 1/2$ according to reaction (10). Below the peritectic temperature, the pseudo-quaternary of ZrSi, $ZrSi_2$, ZrO_2, and SiO_2 explains the reaction couple. Peña [15] reported that although the oxygen diffusion would contribute to the mass balance of the reaction couple, the diffusion path starts at the ZrSi corner which connects with ZrO_2, and then the path traverses to $ZrSi_2$ and finishes at the SiO_2 phase, as shown in Figure 9.

5. PUBLICATIONS AND PARTICIPANTS

Journal publications on the present study are under preparation, and they have been delayed as a result of Professor Bronson's Intergovernmental Personnel assignment at the National Science Foundation. Three presentations were made by students at technical meetings and are listed in Table 3.

Student participants from metallurgical/materials and electrical engineering disciplines were involved in the research. Electrical engineering graduate students included John Kaudeissy, Arturo Duarte, Mariano Olmos, and Gustavo Villalba. Brian Hansen and Sheldon Smith were undergraduate students offering metallurgical/materials engineering support to Maria Peña with her experimental research. Mariano Olmos with his knowledge of control circuits and electromagnetics aided the experimental team in maintaining the induction furnace operational. Brian

Hansen is now enrolled in graduate school at Ohio State University in a doctoral program in materials science and engineering. Three students completed their Masters degree and their names with thesis topics are listed in Table 4.

6. REPORT OF INVENTIONS

No inventions were acquired during the term of the research project.

7. CONCLUSIONS

The finite element analysis (FEA) of the electromagnetic field within the induction furnace determined that the magnetic vector potential was significant just outside the center axis. An energy equation, consisting of the conductive and convective heat transfer equated to the energy generated by the magnetic vector potential, was solved by FEA to determine the temperature distribution within the furnace. The magnetic vector potential can substantially generate a temperature rise within the zirconium disilicide phase because of its conductivity at 1800°C. Although the energy equation did not consider heat losses, which would be substantial at 1800°C, the temperature distribution was consistent with experimental expectations.

A reaction couple of $ZrSi/SiO_2$ was prepared *in-situ* and annealed at temperatures greater than 1900°C. The reaction couple developed an interdiffusion zone near the SiO_2/air interface and an inner core. Within the interdiffusion zone, reaction products consisting ZrO_2 and SiO_2 precipitates resulted from the diffusion of oxygen through a silica layer. During the annealing process, the couple's inner core consisted of ZrSi and liquid silicide, which upon solidification resulted in ZrSi, $ZrSi_2$ and a $Si/ZrSi_2$ eutectic structure.

8. REFERENCES

1. Donea, J.S. Giuliani, and A. Phillipe, "Finite Elements in the Solution of Electromagnetic Induction Problems", International Journal for Numerical Methods in Engineering, vol. 8, pp. 359-367, 1974.

2. E.J.W. Maten and J. B. M. Melissen, "Simulation of Inductive Heating", IEEE Transactions on Magnetics, vol. 28, no. 2, pp. 1287-1290, March 1992.

3. A. Bronson, Y.T. Ma, R. Mutso, and N. Pingitore, "Compatibility of Refractory Metal Boride/Oxide Composites at Ultra High Temperature", The Electrochemical Society Journal, 139, 3183-3196, 1992.

4. J. Davies, and P. Simpson, Induction Heating Handbook, London: McGraw-Hill, 1979.

5. H.A. Sabbagh, "A Model of Eddy-Current Probes with Ferrite Cores", IEEE Transactions on Magnetics, vol. MAG-23, no. 2, pp. 1888-1904, March 1987.

6. S.J. Salon and J. D'Angelo, "Application of the Hybrid Finite Element-Boundary Element Method in Electromagnetics", IEEE Transactions on Magnetics, vol. MAG-24, no. 1, pp. 80-84, January 1988.

7. A. Knoblauch and W. Muller, "Finite Difference Solutions of 3-Dimensional

Eddy-Current Distributions", IEEE Transactions on Magnetics, vol. MAG-19, no. 6, pp. 2393-2396, 1983.

8. M.V.K. Charri, A. Konrad, M. A. Paloma, and J. D'Angelo, "Three-Dimensional Vector Potential Analysis for Machine Field Problems", IEEE Transactions on Magnetics, vol. MAG-18, no. 2, pp. 436-445, March 1982.

9. Y.-H Ko, Finite Element Analysis of Electromagnetic Processing of Refractory Materials, M. S. Thesis, The University of Texas at El Paso, December 1993.

10. G.J. Villalva, Electromagnetic Analysis of an Axisymmetric Induction Heater Using Finite Elements, M. S. Thesis, The University of Texas at El Paso, May 1994.

11. S.P. Murarka, Silicides for VLSI Applications, New York: Academic Press, 1983.

12. G.V. Samsonov, The Oxide Handbook, 2nd Ed., New York: IFI/Plenum, 1982.

13. W.D. Kingery, H. K. Bowen, and D. R. Whymann, Introduction to Ceramics, New York: John Wiley and Sons, 1976.

14. T. B. Massalski, Binary Alloy Phase Diagrams, Second Edition, Vol. 3., ASM International, Metals Park, OH, 1990.

15. M.I. Peña, Ultrahigh Temperature Reactions in a $ZrSi_2/SiO_2$ Diffusion Couple, M.S. Thesis, The University of Texas at El Paso, Metallurgical and Materials Engineering Department, May 1994.

16. E.M. Levin and H.F. McMurdie, Phase Diagrams for Ceramists, American Ceramic Society, Columbus OH, 1975.

Table 1
Material Properties at 1800°C

Region*	Materials of Induction Furnace	σ, Ω-m^2	μ_r	ε_r
1	Carbon dioxide (CO_2)	0	1.0	1.0
2	Zirconium disilicide ($ZrSi_2$)‡	1.94 x $(10)^8$	1.0	1.0
3	Partially Stabilized Zirconia (ZrO_2-10%Y_2O_3)	116.2	1.0	1.0
4	Zirconia Grog (ZrO_2)	20.	1.0	1.0
5	Quartz Reaction Tube (SiO_2)	5.13 x $(10)^{-3}$	1.0	1.0
6	Air	0	1.0	1.0
7	Copper Coil (Cu) #	5.98 x $(10)^8$	1.0	1.0

* Numbers refer to regions of Figure 1
‡ Extrapolated from data provided by Murarka [10] at room temperature and 1000°C.
# Coil is water cooled and a conductivity at 20°C was used.

Table 2.
Summary of X-Ray Diffraction Scans for Samples.

SAMPLE	ZrO_2	ZrO_2	ZrSi	ZrSi	$ZrSi_2$
4 hour					
7 hour	√		√		√
15.9 hour	√	√			
16 hour	√		√	√	√
25 hour	√	√	√	√	√

Table 3
List of Presentations at Symposiums

Authors	Symposiums	Titles
M. I. Peña and A. Bronson	Fall Meeting of The Electrochemical Society, Toronto, Canada. Oxide Films on Metals and Alloys	The Oxidation of Zirconium and Hafnium Silicides
A. Bronson, B. Hansen, J. Pierluissi, Y.-H. Ko	Spring Meeting of The Electrochemical Society, Honolulu, HA	The Electromagnetic Processing of Zirconium Oxide/Silicide Composites
M. I. Peña, B. P. Hansen, A. Bronson	Spring Meeting of The Electrochemical Society, Honolulu, HA	Ultrahigh Temperature Behavior of Zirconium Silicide/Oxide Composites

Table 4
List of Students obtaining Masters Degrees

Students	Thesis Title	Degree, Date, and Department
Yin-Hua Ko	Finite Element Analysis of Electromagnetic Processing of Refractory Materials	Masters, December 1993, Department of Electrical Engineering
Maria I. Peña	Ultrahigh Temperature Reactions in a $ZrSi_2/SiO_2$ Diffusion Couple	Masters, May 1994, Department of Metallurgical and Materials Engineering
G.J. Villalva	Electromagnetic Analysis of an Axisymmetric Induction Heater Using Finite Elements	Masters, May 1994, Department of Electrical Engineering

9. LIST OF FIGURES

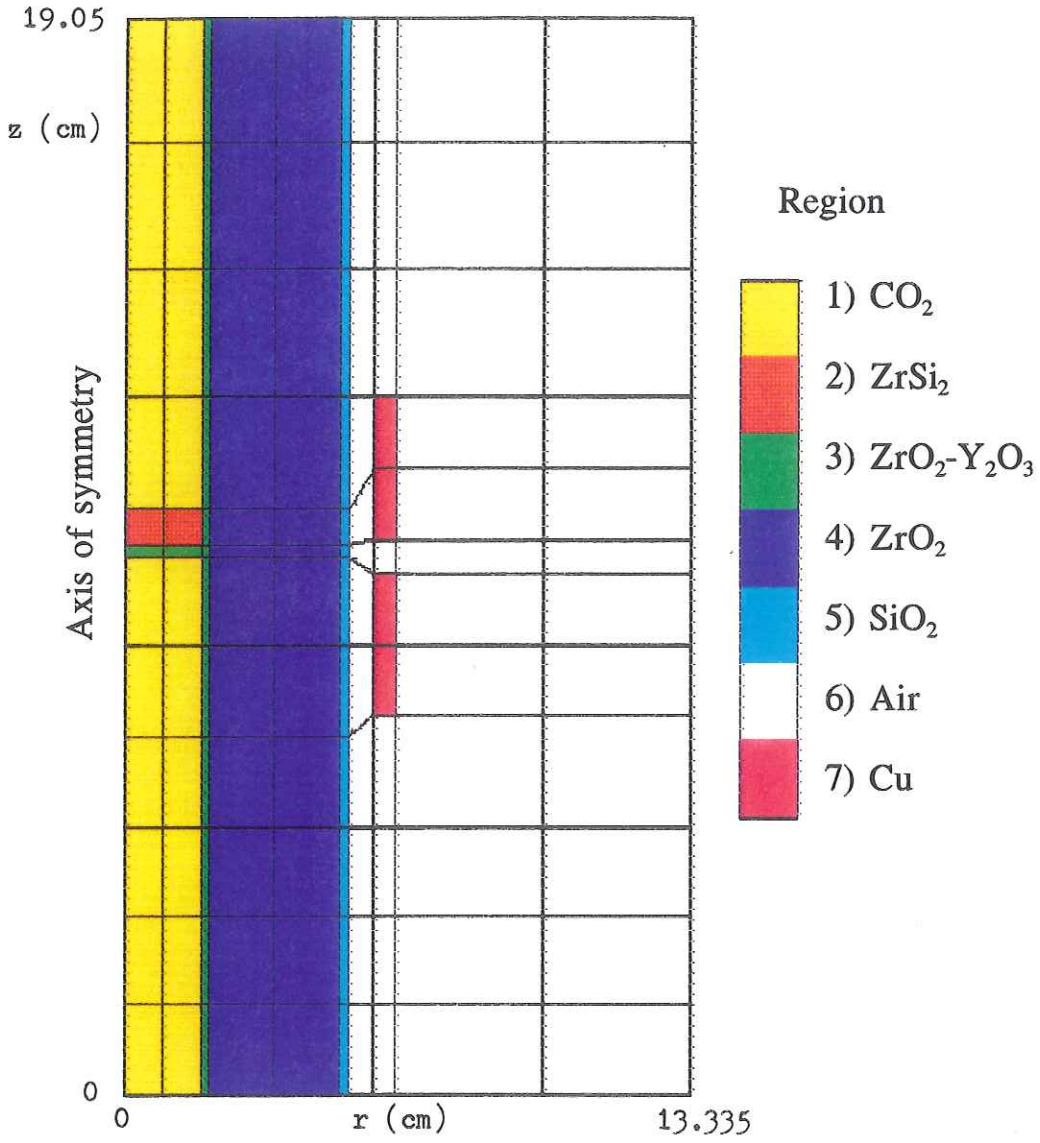

Fig. 1. Composition and finite element mesh for the induction heater.

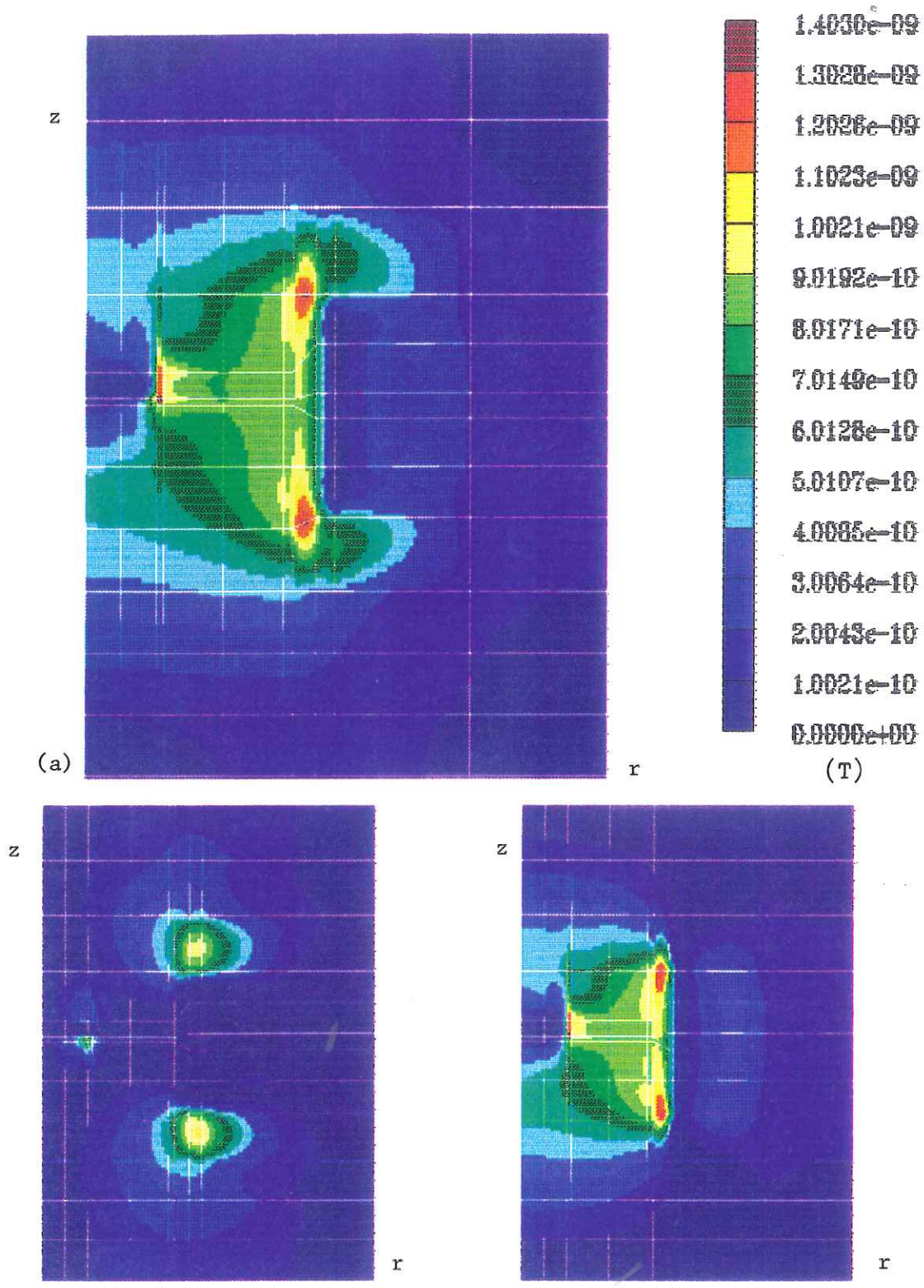

Fig. 2. Magnitudes of the magnetic flux density at 1800 degrees Celsius. (a) Vector. (b) Radial component. (c) Z-component.

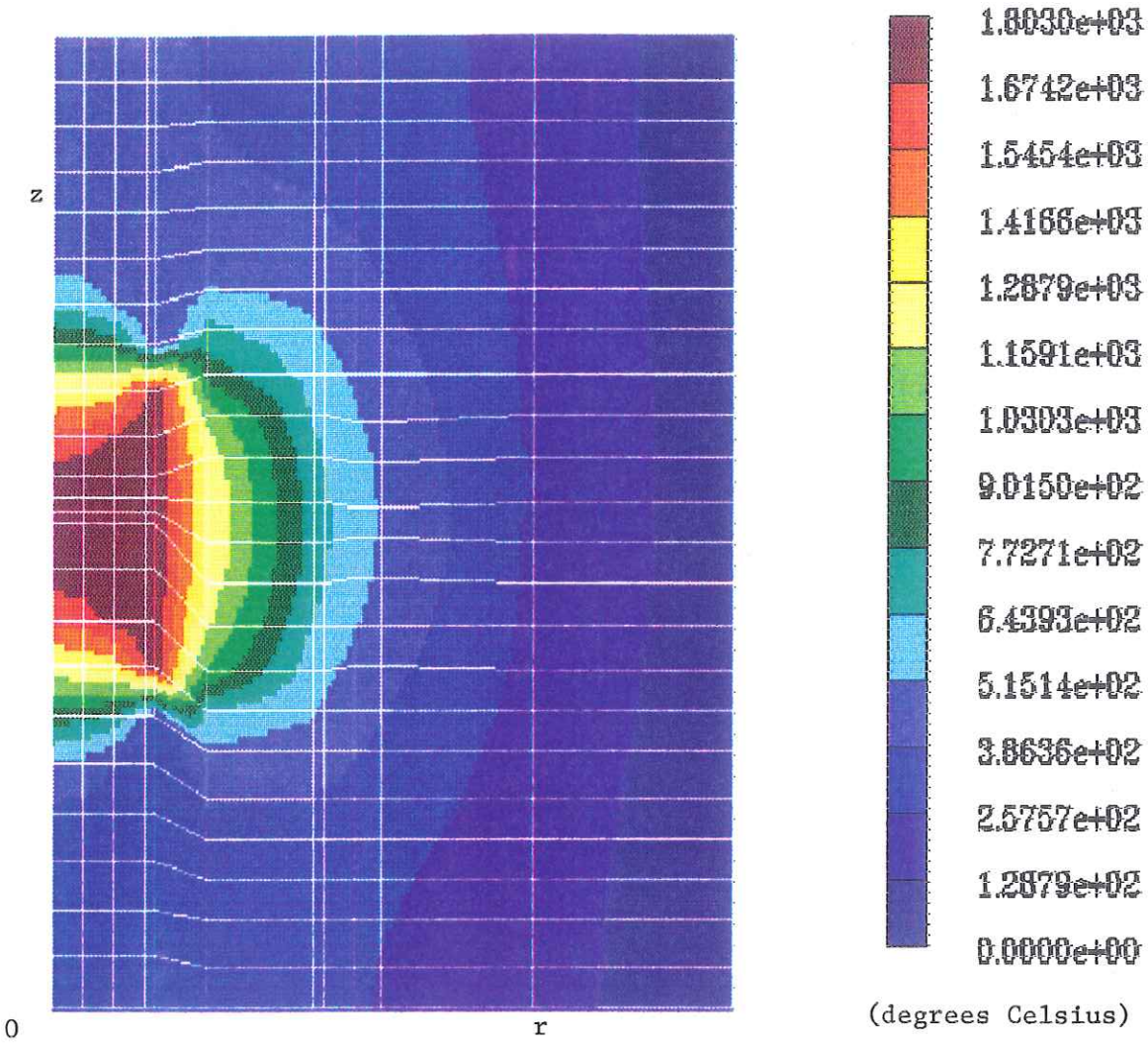

Fig. 3. Temperature profile within the induction furnace at 1800 degrees Celsius.

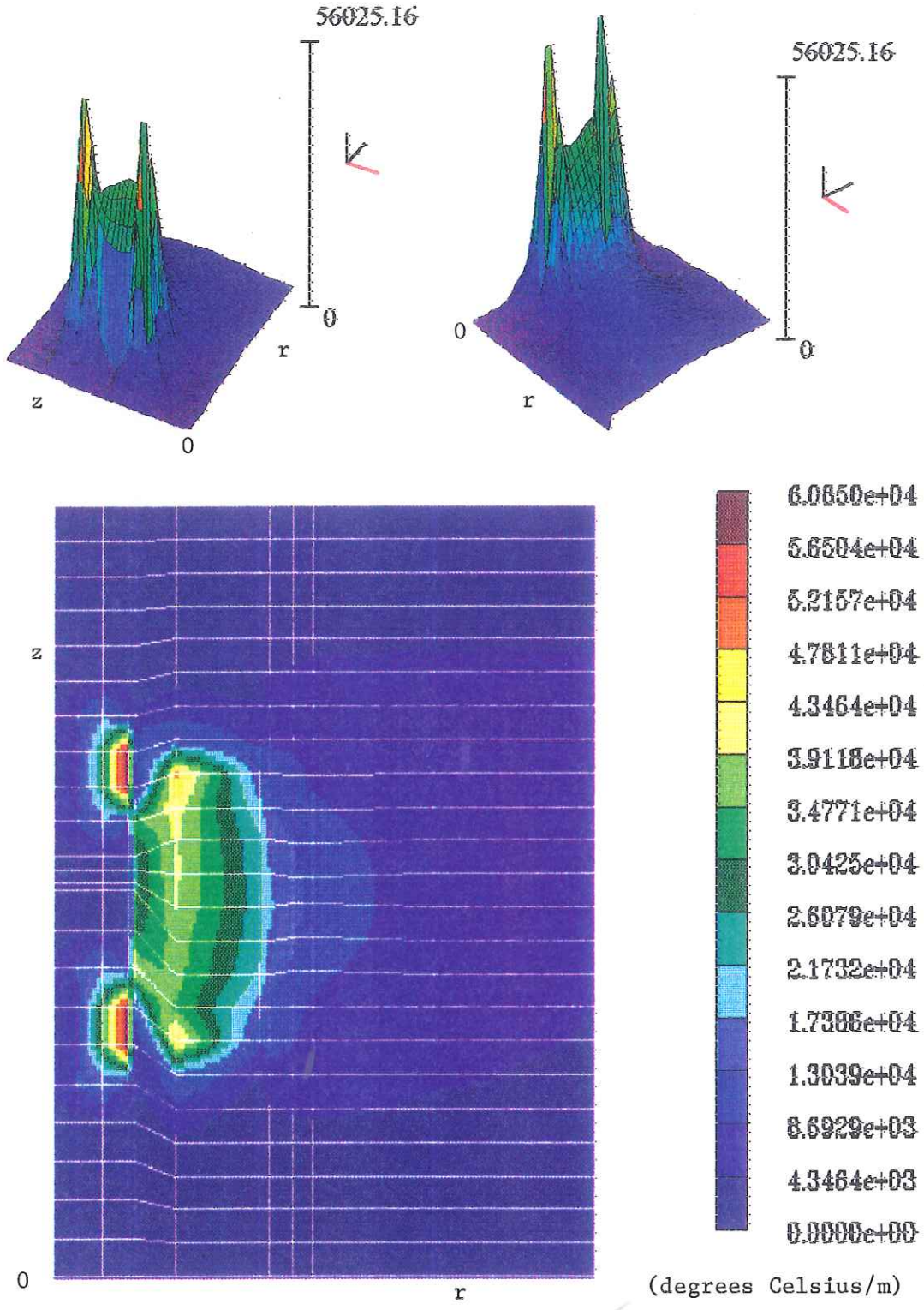

Fig. 4. Temperature gradient in the induction furnace at 1800 degrees Celsius.

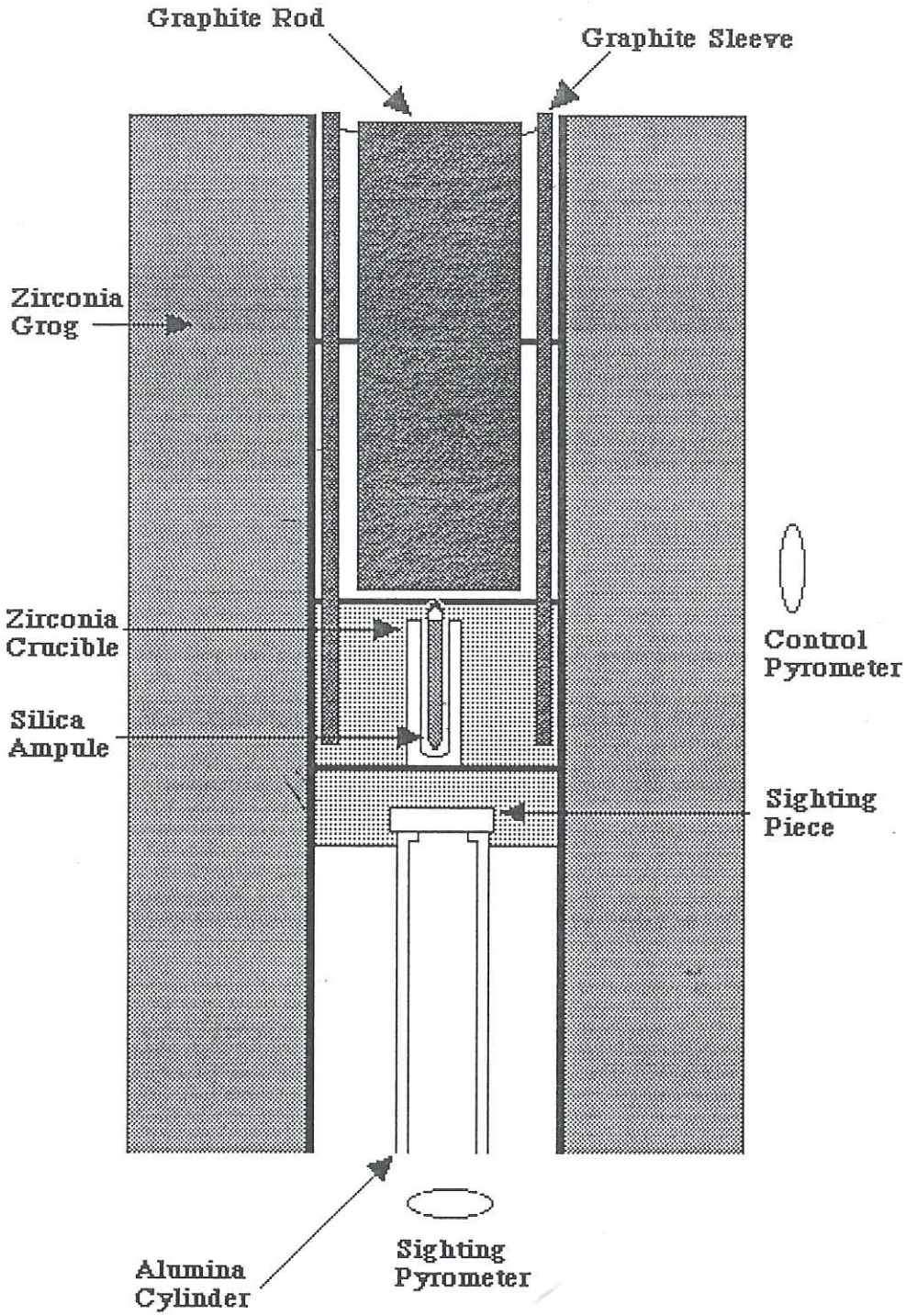

Figure 5 Experimental apparatus showing ampule in zirconia crucible.

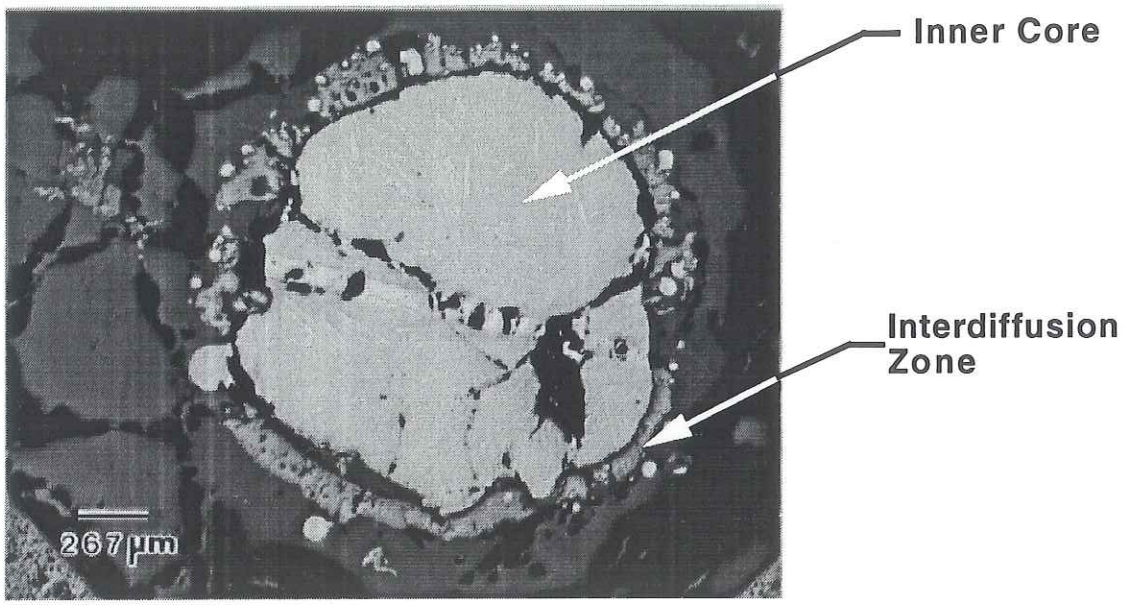

Figure 6 - Optical micrograph of cross-section of the reaction couple.

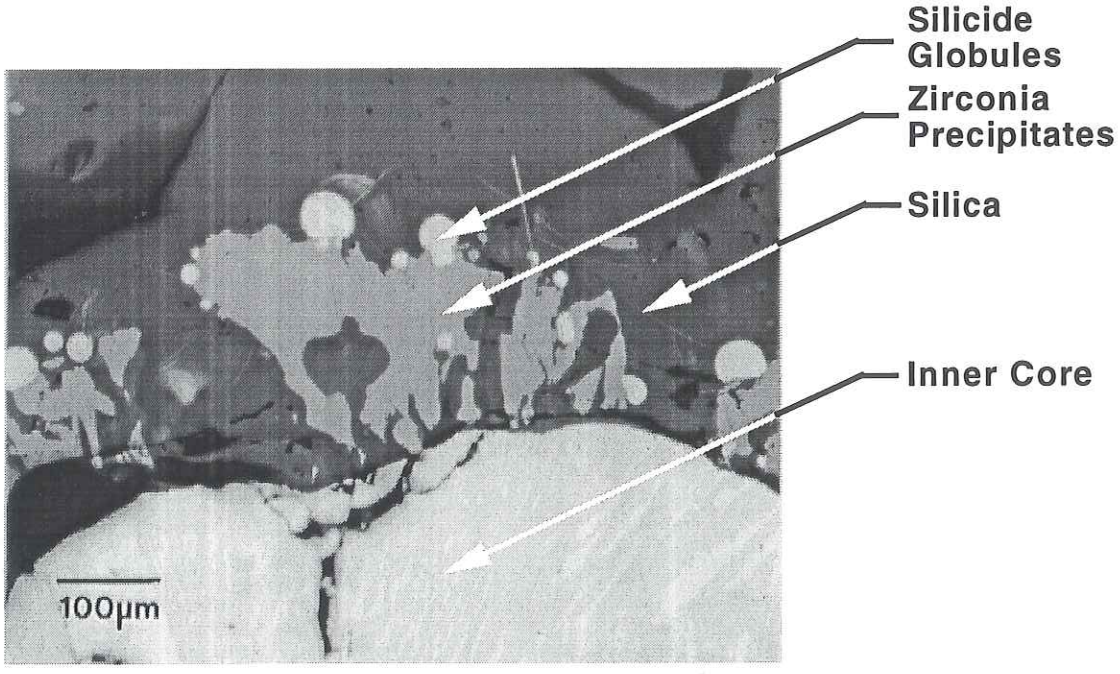

Figure 7 - Scanning electron micrograph of the interdiffusion zone where globules and zirconia precipitates are shown.

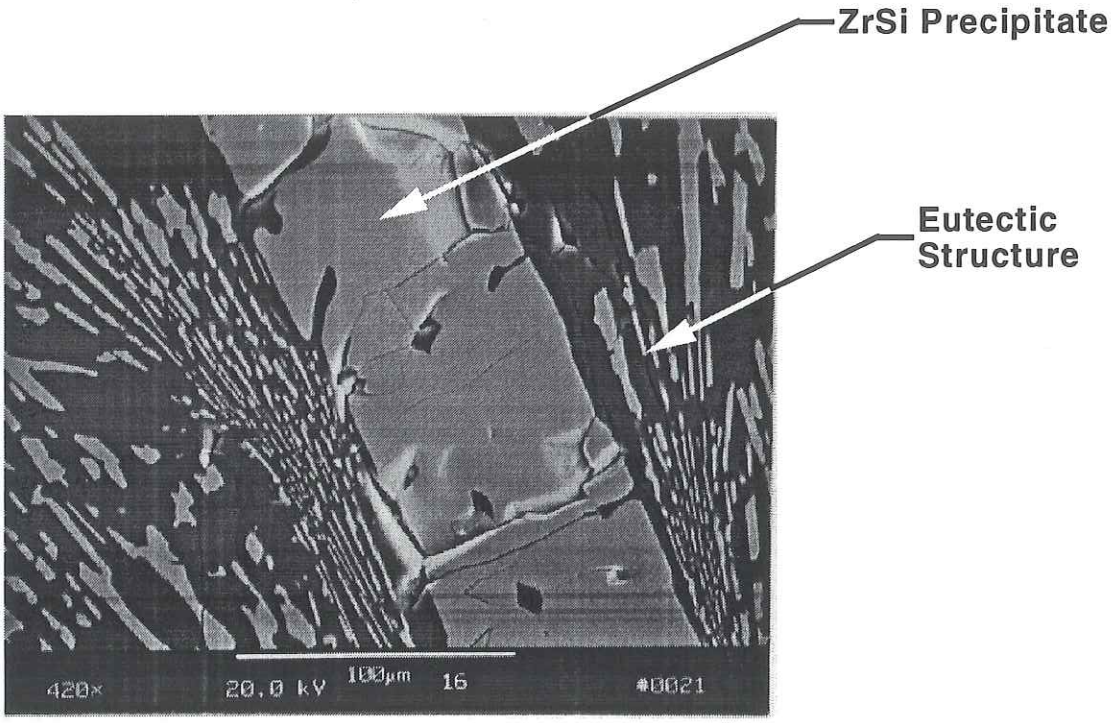

Figure 8 - Scanning electron micrograph of the inner core with a large precipitate and the eutectic structure.

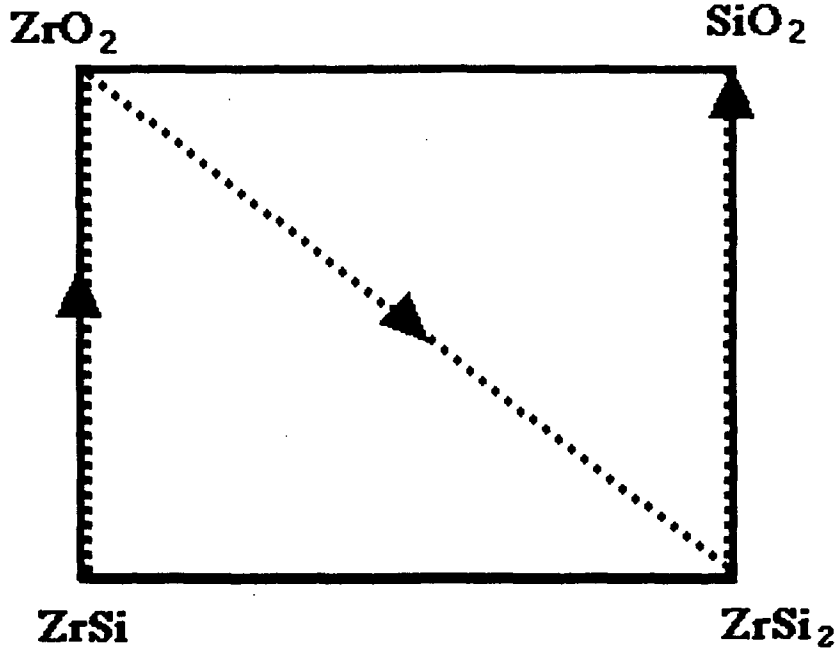

Figure 9 Schematic of the pseudo-quaternary on the elemental ternary with the diffusion path of the reaction couple.